

EQUIVALENT INITIAL FLAW SIZE DISTRIBUTION IN FUSELAGE SKIN SPLICES

S. Fawaz*, J. Lo† and C. Hsu†,

The equivalent initial flaw size (EIFS) distribution and growth of small cracks in four spliced panel configurations representative of transport aircraft fuselage lap joints was investigated as part of the FAA contract on Widespread Fatigue Damage Evaluation for aging aircraft. *In situ* sub-surface crack growth detection and measurement was accomplished using a rotating self-nulling eddy current probe system. Fractographic examination using the scanning electron microscope was employed to determine the crack initiation site, crack shape, and crack history. Corner cracks predominately nucleated at the intersection of the straight portion of the countersunk rivet hole and faying surface. Surface cracks were found which nucleated close to the rivet hole at the faying surface. Once the cracks grew through the sheet thickness, they propagated with part-elliptical crack fronts. The EIFS was determined using FASTRAN and AFGROW.

INTRODUCTION

The Federal Aviation Administration (USA) sponsored an extensive four-year study to investigate the effects of widespread fatigue damage (WFD) on aging aircraft fuselage structure. The program had 6 main thrusts; crack initiation, equivalent initial flaw size (EIFS) distribution, small crack growth, multiple site damage (MSD) in flat panels, WFD in curved panels, and WFD in an aft pressure bulkhead. This paper will focus on only one of the 6 areas, the equivalent initial flaw size distribution.

The crack initiation life and damage tolerance characteristic of splice joints with MSD may vary significantly depending upon the initial size and distribution of the MSD flaws. The statistical behavior of the MSD flaw size and distribution may help explain the scatter in fatigue life and can be used to quantify, in fracture mechanics terms, the quality of the countersunk holes under varying manufacturing techniques and service loading.

The objective of the EIFS study is to generate fractographic data for fatigue cracks nucleating and growing from countersunk fastener holes in the critical row of typical fuselage longitudinal and circumferential splice joints subject to operational loading

* Air Force Research Laboratory, Wright-Patterson Air Force Base, OH USA

† The Boeing Company - Long Beach, California USA

spectra. The observed cracks from the test are then extrapolated backwards using two separate crack growth analysis programs, FASTRAN III and AFGROW; developed by the NASA Langley Research Center and Air Force Research Laboratory, respectively. In addition, a comparison is made between the two crack closure models used in the respective codes. The extrapolation extends from the first observed crack length to the length of the crack at the beginning of the test, time equals zero. To minimize the extrapolation distance, the scanning electron microscope (SEM) is used for post-test fractographic investigation. The EIFS distribution is then assumed to exist in the like structure prior to service and can be accounted for in subsequent damage tolerance analyses.

BACKGROUND

The EIFS concept was first used during the McDonnell Douglas F-4C/D Aircraft Structural Integrity Program (1). In using linear elastic fracture mechanics, the method for determining the EIFS is the same regardless of the crack growth prediction code used. For a given fatigue specimen cycled with a known load history, a portion of the crack growth life can be obtained by *in situ* and/or fractographic measurements. A series of crack growth predictions can then be made with varying initial flaw sizes. The prediction yielding the best correlation between the analysis and experimental data defines the EIFS. If the cracks nucleate and grow as three-dimensional cracks, the crack shape must also be established; thus two parameters must be varied in the predictions, initial flaw size and shape. For example, corner cracks at hole, which are commonly found in mechanically fastened structure, are analyzed by specifying the crack length, c , and the crack depth to crack length ratio, a/c .

The EIFS analyses to follow are a new application of the concept in that two different crack closure models are used. FASTRAN uses a two-parameter plasticity induced closure model where the crack closure is caused by residual plastic deformation remaining in the wake of a growing crack. AFGROW uses a single parameter closure model based on changes in the crack driving force due to the cyclic plastic zone ahead of the crack tip.

EXPERIMENTAL INVESTIGATION

The EIFS specimen panels are based on fuselage splice joint designs that have been used in commercial aircraft for many years. Four types were chosen, two longitudinal lap-splice joints and two butt splice joints, one longitudinal and one circumferential, see Figure 1. All specimens were tested at the Air Force Research Laboratory's wide panel test facility at Wright-Patterson Air Force Base using four computer controlled, closed loop, servo hydraulic load frames. Aluminum doublers were bonded with FM73 to the specimen ends to prevent failure in or near the grip area. The overall specimen dimensions are 559 mm x 1422 mm with 559 mm x 1118 mm outside the grip area; thus the specimen length to width ratio (L/W) is 2.0. An L/W of 2.0 was chosen to ensure a uniform stress distribution through the width of the specimen outside the joint overlap

region. Three different load spectra were used in attempt to mark the fracture surface with marker bands to aid crack growth history reconstruction via fractographic analysis. Marker bands are created by an instantaneous or short duration variation in the constant amplitude (CA) maximum stress or stress ratio, which perturb the fatigue striation spacing created by the CA loading. The first spectrum contained 2000 baseline CA cycles with $S_{\max} = 103.4$ MPa and $R = 0.02$ followed by 10 overload cycles with $S_{\max} = 134.5$ MPa and $R = 0.02$. The second spectrum contains 1000 baseline CA cycles followed by periodic blocks of 100 CA cycles at $S_{\max} = 77.6$ MPa, $R = 0.02$ and 10 baseline CA cycles, further details of this spectrum can be found in (2). The third spectrum is a transport aircraft fuselage flight spectrum developed by The Boeing Company (3).

Crack detection and measurement was accomplished using the rotating self-nulling eddy current probe system (RPS) for subsurface cracks, cracks growing under the countersunk rivet head (4). A traveling optical microscope (TOM) mounted on a linear voltage displacement transducer (LVDT) was attached to the load frame to measure the cracks once they grew through the specimen thickness. After specimen failure, the critical rivet row, the rivet row containing the cracks that ultimately caused specimen failure, was removed and each crack was cut out for fractographic investigation in the SEM.

Wide panel testing not only offers a more realistic representation of the full-scale structure, but may also respond to static or dynamic loading differently than the full-scale structure. The joints tested here differ from the real structure in that the specimen edges are unconstrained and in a fuselage circumferential and longitudinal stiffeners, frames and stringers, restrain the skin. This lack of restraint allows for an increased rotation about the joint and longitudinal axes of the specimen resulting in higher secondary bending stresses at the edges. Furthermore, the increased stiffness of the specimen in the joint overlap area, boxed area in Figure 1, constricts the amount of poisson contraction in the overlap area compared to the skin. Thus, rivet loads at the specimen edge are larger than those of the interior rivets in the same row. Unfortunately, the larger secondary bending stresses and rivet loads cause edge cracking, cracks that nucleate and grow at the rivet holes in the outer rivet rows closest to the specimen edge. Due to the high crack driving force of an edge cracked rivet hole, MSD cannot develop in the remaining rivets of the same row. Several researchers have prevented edge cracking by stop drilling (5), use of oversized rivets (5), ball indentation at the crack tip (6), use of protruding head rivets (7,8), and application of doublers at the specimen edge (7,8). Four different methods were used in this study as shown in Figure 2. One, from the specimen edge to the first column of rivets for all specimens, the skins were bonded together using FM73. Two, edge clamps were placed over the first (and last) column of rivets. Three, the skin material outside the joint was cut into a dog-bone shape. Four, the first column of rivets at the specimen edge were oversized and heavily expanded.

RESULTS AND DISCUSSION

A total of 16 specimens were tested, four of each joint type, with fatigue crack growth data obtained from 12 specimens. Bonding of the skin at the specimen edges was completely insufficient resulting in edge cracking of one type I joint. A second type I joint experienced edge cracking due to an improperly designed edge block which allowed

contact between the edge block and skin outside the joint area. The specimen failed due to a crack in the skin initiated by fretting. The remaining type I joints were tested successfully with redesigned edge blocks with row C being the critical rivet row. The type II joints were tested with edge blocks and row A was the critical rivet row. Edge blocks did not preclude edge cracking in the type III joints although the secondary bending was lower at the specimen edge than center. The stiffness of the overlap area in the type III (and IV) joints is greater than in the types I and II where the edge blocks prohibited edge cracking. This suggests the restriction of the poisson contraction at the outer rivet rows, and the subsequent higher rivet loads is causing the edge cracking. The dog-bone shape of the skin outside the joint reduces the amount of load transferred by the rivets at the specimen edge. Care must be taken in designing the dog-bone notch since the stress concentration, K_T , may cause failure at the notch root, r . Indeed, when the $r = 63.5$ mm, $K_T = 1.75$ failure was at the notch root; whereas when $r = 495$ mm, $K_T = 1.3$ failure was in the critical rivet row. Using the larger notch root radius, edge cracking was prevented in the type III joints, and the outer rivet rows, A or F, were critical. The critical rivet row in the type IV joint was row D. The dog-boned skin does not reduce the rivet loading for rows D and E of the type IV joint. In order to prevent edge cracking, the outer column rivets were removed and replaced with the next oversized rivet, and the driven head was expanded until it was 1.8 times the original shank diameter. Three of the four type IV joints had dog-boned skins along with the larger rivets. The last type IV joint was tested with only the highly expanded outer column rivets demonstrating the effectiveness of using a high rivet squeeze force to keep cracks from nucleating.

Fractographic Analysis

The spectrum with the 130% overload did not adequately mark the fracture surface since the change in the effective stress intensity factor during the overload cycles was insufficient. The second spectrum used created marker bands through final fracture and to crack lengths as small as $9 \mu\text{m}$. The transport aircraft flight spectrum also effectively marked the fracture surface enabling post-test crack growth history reconstruction via the SEM.

Fatigue Crack Growth Predictions

Predictions for one type II joint have been completed using FASTRAN and AFGROW. The predictions show good correlation with the test data. The EIFS determined using FASTRAN and AFGROW was $3.6 \mu\text{m} \leq c_i \leq 29.2 \mu\text{m}$ and $18 \mu\text{m} \leq c_i \leq 27 \mu\text{m}$, respectively, as seen in Figure 3. Based on fractographic observations from the present study and reference (2), the initial crack shape was quarter circular, $a/c = 1.0$. Interestingly, the smallest FASTRAN determined EIFS ($3.6 \mu\text{m}$) is below the lower limit of initial crack sizes found by Newman and Edwards (9) which suggests this particular EIFS has no physical basis. Both prediction codes require input of normalized stresses (stress ratios) for each load condition. Thus, the bypass, bending, and bearing stresses are all normalized by the remote applied tensile stress, which was 103.4 MPa. The resulting

stress ratios are 0.654, 0.395, and 1.978 for bypass, bending and bearing, respectively. The effects of rivet interference, friction between contact surfaces, and load shedding have been combined in a correlation factor as a function of the faying surface crack length (10).

CONCLUSION

Four different transport aircraft fuselage flat panel skin joints were successfully fatigue tested under operational loading spectra. Edge cracking in the joints was eliminated by cutting a dog-bone shape in the skins and over-sizing and -expanding the rivets at the specimen edges, first and last column of rivets. The fatigue critical rivet row(s) for joint type I was row C, joint types II and III were the outer rows, and joint type IV were the inner most rows. The equivalent initial flaw size using the crack closure model in FASTRAN and AFGROW was $3.6 \mu\text{m} \leq c_i \leq 29.2 \mu\text{m}$ and $18 \mu\text{m} \leq c_i \leq 27 \mu\text{m}$, respectively.

REFERENCES

-
- (1) Rudd, J. and Gray, T., "Equivalent Initial Quality Method," AFFDL-TM-76-83-FBE, 1976.
 - (2) Fawaz, S., Schijve, J., and de Koning, A., "Fatigue Crack Growth in Riveted Lap-Splice Joints," Proc. of the 19th ICAF Symposium, EMAS, Scotland, UK, 1997.
 - (3) Yu, J., "Equivalent Initial Flaw Size Study Test Plan," The Boeing Company, USA, 1997.
 - (4) Hagemaijer, D., "Eddy Current Detection of Short Cracks Under Installed Fasteners." Materials Evaluation, 55, No. 1, 1997.
 - (5) Wit, G., MSD in Fuselage Lap Joints - Requirements for Inspection Intervals for Typical Fuselage Lap Joint Panels with Multiple Site Damage, LR-697, Delft Univ. of Tech., 1992.
 - (6) Vlieger, H. Results of Uniaxial and Biaxial Tests on Riveted Fuselage Lap Joint Specimens, Hampton, VA, NASA-CP-3274, 1994.
 - (7) Mayville, R. and Warren, T. "A Laboratory Study of Fracture in the Presence of Lap Splice Multiple Site Damage," Eds. S. N. Atluri, S. G. Sampath, and P. Tong. Structural Integrity of Aging Airplanes, Springer Series in Computational Mechanics. Berlin: Springer Verlag, 1991.
 - (8) Eastaugh, G., Simpson, D., Straznicki, P., and Wakeman, R. "A Special Uniaxial Coupon Test Specimen for the Simulation of Multiple Site Fatigue Crack Growth and Link-Up in Fuselage Skin Splices," AGARD-CP-568. Neuilly-Sur-Seine, Fr. 1995.
 - (9) Newman Jr., J. C. and Edwards, P. R., "Short-Crack Growth Behaviour in an Aluminum Alloy- An AGARD Cooperative Test Programme," AGARD-R-732, 1988.
 - (10) Hsu, J. and Yu, J., "Initial Quality of Typical Aircraft Fuselage Splice Joints Investigated in WFD Program," Proc. of ICES, Atlanta, GA, 1998.

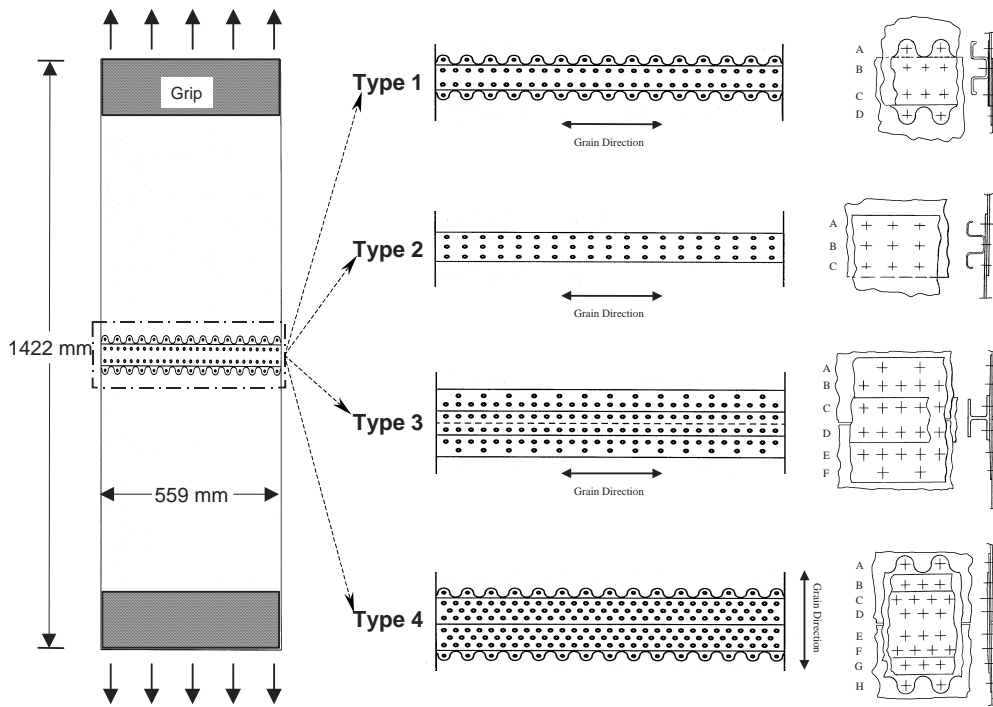


Figure 1 Equivalent Initial Flaw Size Joint Types

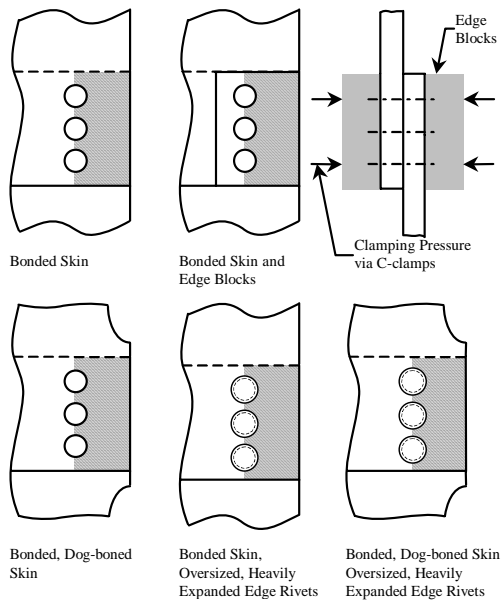


Figure 2 Methods for Preventing Edge Cracking in Wide Panel Fatigue Tests

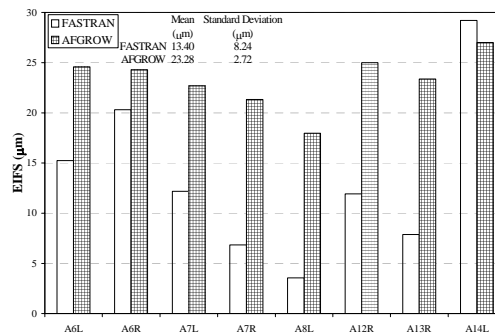


Figure 3 EIFS Determination Using FASTRAN III and AFGROW